An Adaptive Controller for Two Cooperating Flexible Manipulators

C. J. Damaren[1]

[1]University of Toronto, Institute for Aerospace Studies, 4925 Dufferin Street, Toronto, Ontario, M3H 5T6, CANADA
cjd@sdr.utias.utoronto.ca

Abstract

The control problem for two serial flexible multilink robots which carry a common rigid payload is considered. An adaptive controller with feedback and feedforward elements is presented which can track a prescribed trajectory for the payload with simultaneous vibration suppression when the manipulated payload is sufficiently large.

1. Introduction

The adaptive control of robot manipulators has been presented as a solution for dealing with uncertainty and variation of the mass properties. Although these systems are nonlinear, globally stable tracking has been demonstrated both analytically and supported through experiments [1]. The key to these results has been the linear dependence of the model on the unknown parameters and, in many cases, the passivity of an appropriate input-output mapping [2]. For instance, with rigid robots it is well known that the map from joint torques to joint rates is passive and this property can be used to explain the stabilization properties of many motion control strategies including the ubiquitous proportional-derivative position feedback.

Motivated by the utility of the passivity concept in rigid robot control and its occurrence in a single flexible link when the reflected tip rate is taken as the output [3], the present author introduced the μ-tip rate in [4] which generalized this output to open-chain flexible manipulators. Passivity using this output was demonstrated for $\mu < 1$ when the manipulated payload was much more massive than the manipulator and a feedforward which permitted its use in tracking problems was constructed in [5]. The adaptive counterpart of that controller was detailed in [6] and variations of both controllers were implemented experimentally with great success in [7].

The extension of the μ-tip rate idea to cooperating robot arms forming a closed chain was treated in [8] where detailed stability proofs and experimental results were presented. An interesting feature of this development was the occurrence of a free-loading sharing parameter which was used to distribute the control torques between the two arms and form the generalization of the μ-tip rate. Beyond this, the dynamics and control of cooperating flexible arms has received little attention but there has been some [9,10]. This paper represents the dénouement for the line of research pursued in [4-8]. A fusion of the previous techniques is brought to bear on the problem of adaptive control for cooperating flexible robot arms in the case where the payload is significantly larger than the manipulators but otherwise unknown.

Simulation results will be presented for a system of two planar arms each with three joints that manipulate a shared rigid payload. Each arm has two flexible links and a third rigid link which is cantilevered to the large rigid payload. Excellent tracking is demonstrated with simultaneous vibration suppression for the adaptive controller when the payload is sufficiently large for a variety of load-sharing parameters.

2. Cooperating Flexible Robots

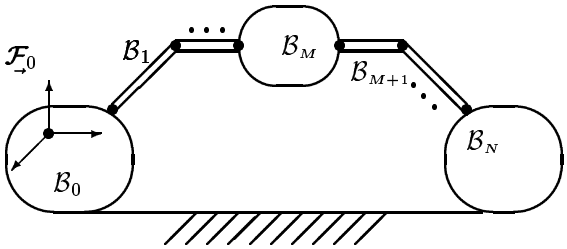

Figure 1: Closed-Loop Multibody System

This work deals with a chain of flexible and/or rigid bodies as shown in Figure 1. Bodies $\mathcal{B}_0$ and $\mathcal{B}_N$ are cantilevered in an inertial reference frame $\mathcal{F}_0$ so as to form a closed loop. The bodies are connected by revolute joints and $\boldsymbol{\theta} = \text{col}\{\theta_n\}$, $n = 1 \cdots N$, denotes the collection of joint angles and $\mathbf{q}_e = \text{col}\{\mathbf{q}_{en}\}$ is the collection of N_e elastic degrees of freedom.

The body $\mathcal{B}_M$, $1 \leq M \leq N$, is taken to be a rigid payload under manipulation and it is assumed that M

is equal to the number of rigid degrees of freedom after loop closure. The joint angles and elastic coordinates are further partitioned as

$$\begin{aligned}\boldsymbol{\theta}_1 &= \text{col}\{\theta_n\}, n = 1, \cdots, M, &(1)\\ \boldsymbol{\theta}_2 &= \text{col}\{\theta_n\}, n = M+1, \cdots, N, &(2)\\ \mathbf{q}_{1e} &= \text{col}\{\mathbf{q}_{en}\}, n = 1, \cdots, M, &(3)\\ \mathbf{q}_{2e} &= \text{col}\{\mathbf{q}_{en}\}, n = M+1, \cdots N. &(4)\end{aligned}$$

The payload position $\boldsymbol{\rho}$ is interpreted as a six-tuple whose top half contains the position of $\mathcal{B}_M$ with respect to $\boldsymbol{\mathcal{F}}_0$ and whose bottom half is an attitude parametrization such as Euler angles.

The payload position can be written as $\boldsymbol{\rho} = \boldsymbol{\mathcal{F}}_1(\boldsymbol{\theta}_1, \mathbf{q}_{e1}) = \boldsymbol{\mathcal{F}}_2(\boldsymbol{\theta}_2, \mathbf{q}_{e2})$ where $\boldsymbol{\mathcal{F}}_i$, $i = 1, 2$, are the forward kinematics maps. Its velocity is given by

$$\dot{\boldsymbol{\rho}} = \boldsymbol{J}_{i\theta}(\boldsymbol{\theta}_i, \mathbf{q}_{ie})\dot{\boldsymbol{\theta}}_i + \boldsymbol{J}_{ie}(\boldsymbol{\theta}_i, \mathbf{q}_{ie})\dot{\mathbf{q}}_{ie},\ i = 1, 2, \quad (5)$$

where $\boldsymbol{J}_{i\theta}$, $\boldsymbol{J}_{ie}$, $i = 1, 2$, are the corresponding Jacobian matrices. The μ-tip rate described in Sec. 1 is defined by

$$\begin{aligned}\dot{\boldsymbol{\rho}}_\mu &= \mu\dot{\boldsymbol{\rho}} + (1-\mu)[C_1\boldsymbol{J}_{1\theta}\dot{\boldsymbol{\theta}}_1 + C_2\boldsymbol{J}_{2\theta}\dot{\boldsymbol{\theta}}_2] &(6)\\ &= \dot{\boldsymbol{\rho}} - (1-\mu)[C_1\boldsymbol{J}_{1e}\dot{\mathbf{q}}_{1e} + C_2\boldsymbol{J}_{2e}\dot{\mathbf{q}}_{2e}] &(7)\end{aligned}$$

where C_1 with $0 < C_1 < 1$ and $C_2 = 1 - C_1$ will be termed *load-sharing parameters*. For $\mu = 1$, $\boldsymbol{\rho}_\mu = \boldsymbol{\rho}$, the true payload position, while for $\mu = 0$, $\boldsymbol{\rho}_\mu$ describes an output based on the joint motion alone. If the approximations $\boldsymbol{J}_{i\theta}(\boldsymbol{\theta}_i, \mathbf{q}_{ie}) \doteq \boldsymbol{J}_{i\theta}(\boldsymbol{\theta}_i, \mathbf{0})$, $i = 1, 2$, are made then the integral of (6) yields $\boldsymbol{\rho}_\mu(t) = \mu\boldsymbol{\rho}(t) + (1-\mu)[C_1\boldsymbol{\mathcal{F}}_1(\boldsymbol{\theta}_1, \mathbf{0}) + C_2\boldsymbol{\mathcal{F}}_2(\boldsymbol{\theta}_2, \mathbf{0})]$ where $\boldsymbol{\mathcal{F}}_i(\boldsymbol{\theta}_i, \mathbf{0})$ are the rigid forward kinematical maps. The control torques are assumed to be determined according to

$$\boldsymbol{\tau} = [\tau_1\ \cdots\ \tau_N]^T = [C_1\boldsymbol{J}_{1\theta}\quad C_2\boldsymbol{J}_{2\theta}]^T\widehat{\boldsymbol{\tau}} \quad (8)$$

where $\widehat{\boldsymbol{\tau}}$ is a collection of M control inputs; hence the load-sharing description for the C_i. The paper establishes a control scheme for $\boldsymbol{\tau}(t)$ so that $\boldsymbol{\rho}(t)$ tracks a prescribed payload trajectory $\boldsymbol{\rho}_d(t)$.

3. Large Payload Dynamics

In [8], it was established that the dynamics of the closed-loop flexible robot under the assumption that $\mathcal{B}_M$ was large were described by

$$\begin{aligned}\boldsymbol{M}_{\rho\rho}\ddot{\boldsymbol{\rho}} + \boldsymbol{C}_\rho(\boldsymbol{\rho}, \dot{\boldsymbol{\rho}})\dot{\boldsymbol{\rho}} &= \widehat{\boldsymbol{\tau}}, &(9)\\ \boldsymbol{C}_\rho(\boldsymbol{\rho}, \dot{\boldsymbol{\rho}})\dot{\boldsymbol{\rho}} = \dot{\boldsymbol{M}}_{\rho\rho}\dot{\boldsymbol{\rho}} &- \tfrac{1}{2}\partial(\dot{\boldsymbol{\rho}}^T\boldsymbol{M}_{\rho\rho}\dot{\boldsymbol{\rho}})/\partial\boldsymbol{\rho}, &(10)\\ \widehat{\boldsymbol{M}}_{ee}\ddot{\mathbf{q}}_e + \mathbf{D}_{ee}\dot{\mathbf{q}}_e &+ \mathbf{K}_{ee}\mathbf{q}_e = \\ &- [C_1\boldsymbol{J}_{e1}\ C_2\boldsymbol{J}_{e2}]^T\widehat{\boldsymbol{\tau}}. &(11)\end{aligned}$$

In the first of these, $\boldsymbol{M}_{\rho\rho}$ is the task-space mass matrix of the equivalent rigid arm evaluated at $\boldsymbol{\theta}_i = \boldsymbol{\mathcal{F}}_{ri}^{-1}(\boldsymbol{\rho})$ where $\boldsymbol{\mathcal{F}}_{ri}^{-1}(\cdot)$, $i = 1, 2$, are the rigid inverse kinematics maps. Hence, (9) and (10) are equivalent to the rigid-body *task-space* motion equations. In the second equation, $\widehat{\boldsymbol{M}}_{ee} = \widehat{\boldsymbol{M}}_{ee}^T > \mathbf{O}$ is the mass matrix relative to $\mathbf{q}_e$ assuming that the large payload forms a clamping boundary condition ($\boldsymbol{\rho} = \mathbf{0}$) and $\boldsymbol{K}_{ee} = \boldsymbol{K}_{ee}^T > \mathbf{O}$ is the stiffness matrix. We have added a damping term $\boldsymbol{D}_{ee}\dot{\mathbf{q}}_e$ with $\boldsymbol{D}_{ee} = \boldsymbol{D}_{ee}^T > \mathbf{O}$ which is required in the stability proof in the adaptive case.

A further simplification is possible if one includes only the payload contributions to $\boldsymbol{M}_{\rho\rho}$. First, recognize that in this case (9) is equivalent to the motion equation for a single rigid body with kinetic energy $(1/2)\dot{\boldsymbol{\rho}}^T\boldsymbol{M}_{\rho\rho}\dot{\boldsymbol{\rho}} = (1/2)\boldsymbol{\nu}^T\boldsymbol{M}\boldsymbol{\nu}$ where

$$\boldsymbol{M} = \begin{bmatrix} m\mathbf{1} & -\mathbf{c}^\times \\ \mathbf{c}^\times & \mathbf{J}\end{bmatrix},\ \boldsymbol{\nu} = \begin{bmatrix}\mathbf{v}\\ \boldsymbol{\omega}\end{bmatrix}.$$

Here, $\boldsymbol{\nu}$ is the generalized velocity of the payload body expressed in a body-fixed frame consisting of the translational velocity $\mathbf{v}$ in the top three-tuple and the angular velocity $\boldsymbol{\omega}$ in the bottom. $\boldsymbol{M}$ is the corresponding (constant) mass matrix containing the zeroth (m), first ($\mathbf{c}$), and second ($\mathbf{J}$) moments of mass. Note that $\boldsymbol{\nu} = \boldsymbol{P}(\boldsymbol{\rho})\dot{\boldsymbol{\rho}}$ where $\boldsymbol{P} = \text{diag}\{\mathbf{C}_{M0}(\boldsymbol{\rho}), \mathbf{S}_{M0}(\boldsymbol{\rho})\}$, $\mathbf{C}_{M0}$ is the rotation matrix describing the orientation of $\mathcal{B}_M$ with respect to $\boldsymbol{\mathcal{F}}_0$, and $\mathbf{S}_{M0}$ is the corresponding matrix transforming Euler rates into (body-frame) angular velocity. To facilitate the subsequent development, the six-dimensional extension of the cross-operator is defined by

$$\boldsymbol{\nu}^\otimes = \begin{bmatrix}\boldsymbol{\omega}^\times & \mathbf{O}\\ \mathbf{v}^\times & \boldsymbol{\omega}^\times\end{bmatrix},\ \boldsymbol{\nu}^T\boldsymbol{\nu}^\otimes = \mathbf{0}.$$

The notation $(\cdot)^\times$ denotes the 3×3 skew-symmetric matrix used to implement the vector cross product. The motion equation (9) can now be written in the form

$$\boldsymbol{M}\dot{\boldsymbol{\nu}} + \boldsymbol{\nu}^\otimes\boldsymbol{M}\boldsymbol{\nu} = \boldsymbol{P}^{-T}(\boldsymbol{\rho})\widehat{\boldsymbol{\tau}}. \quad (12)$$

4. The Adaptive Controller

The desired trajectory is prescribed by $\{\boldsymbol{\rho}_d, \dot{\boldsymbol{\rho}}_d, \ddot{\boldsymbol{\rho}}_d\}$ and it is assumed that $\boldsymbol{\rho}_d \to \bar{\boldsymbol{\rho}}_d$ (constant) as $t \to \infty$. The following quantities play an essential role:

$$\begin{aligned}\boldsymbol{\nu}_d &= \boldsymbol{P}(\boldsymbol{\rho})\dot{\boldsymbol{\rho}}_d,\\ \widetilde{\boldsymbol{\nu}} &= \boldsymbol{\nu} - \boldsymbol{\nu}_d = \boldsymbol{P}(\boldsymbol{\rho})\dot{\widetilde{\boldsymbol{\rho}}},\ \widetilde{\boldsymbol{\rho}} = \boldsymbol{\rho} - \boldsymbol{\rho}_d,\\ \boldsymbol{\nu}_r &= \boldsymbol{\nu}_d - \boldsymbol{P}(\boldsymbol{\rho})\boldsymbol{\Lambda}\widetilde{\boldsymbol{\rho}}_\mu = \boldsymbol{P}(\boldsymbol{\rho})[\dot{\boldsymbol{\rho}}_d - \boldsymbol{\Lambda}\widetilde{\boldsymbol{\rho}}_\mu],\\ \widetilde{\boldsymbol{\rho}}_\mu &= \boldsymbol{\rho}_\mu - \boldsymbol{\rho}_{\mu d}, &(13)\end{aligned}$$

$$\widetilde{\boldsymbol{\nu}}_r = \boldsymbol{\nu} - \boldsymbol{\nu}_r = \boldsymbol{P}(\boldsymbol{\rho})[\dot{\widetilde{\boldsymbol{\rho}}} + \boldsymbol{\Lambda}\widetilde{\boldsymbol{\rho}}_\mu], \quad (14)$$

$$\mathbf{s}_\mu = \dot{\widetilde{\boldsymbol{\rho}}}_\mu + \boldsymbol{\Lambda}\widetilde{\boldsymbol{\rho}}_\mu, \quad (15)$$

where $\boldsymbol{\Lambda} = \boldsymbol{\Lambda}^T > \mathbf{O}$ and $\boldsymbol{\rho}_{\mu d}$ is the desired form of $\boldsymbol{\rho}_\mu$ discussed below. Given the structure of the payload motion equation (12), our choice of feedforward torque can be written as

$$\boldsymbol{P}^{-T}\widehat{\boldsymbol{\tau}}_d = \boldsymbol{W}(\dot{\boldsymbol{\nu}}_r, \boldsymbol{\nu}_r, \boldsymbol{\nu})\mathbf{a} \triangleq \boldsymbol{M}\dot{\boldsymbol{\nu}}_r + \boldsymbol{\nu}_r^{\otimes}\boldsymbol{M}\boldsymbol{\nu} \quad (16)$$

where $\mathbf{a} = \mathrm{col}\{m, \mathbf{c}, \mathbf{j}\}$ ($\mathbf{j}$ is a column of the six independent moment of inertia elements) and $\boldsymbol{W}$ is termed the regressor matrix.

The desired behaviour for the elastic displacements, $\mathbf{q}_{ed}$, is defined by

$$\widehat{\boldsymbol{M}}_{ee}\ddot{\mathbf{q}}_{ed} + \mathbf{D}_{ee}\dot{\mathbf{q}}_{ed} + \mathbf{K}_{ee}\mathbf{q}_{ed} = - [C_1\boldsymbol{J}_{1e}\ C_2\boldsymbol{J}_{2e}]^T\widehat{\boldsymbol{\tau}}_d \quad (17)$$

and the desired form of $\boldsymbol{\rho}_\mu$ is defined by $\dot{\boldsymbol{\rho}}_{\mu d} = \dot{\boldsymbol{\rho}}_d - (1-\mu)[C_1\boldsymbol{J}_{1e}\dot{\mathbf{q}}_{1e,d} + C_2\boldsymbol{J}_{2e}\dot{\mathbf{q}}_{2e,d}]$. Subtracting (16) from (12) and (17) from (11) yields the following form of the error dynamics:

$$\boldsymbol{M}\dot{\widetilde{\boldsymbol{\nu}}}_r + \widetilde{\boldsymbol{\nu}}_r^{\otimes}\boldsymbol{M}\boldsymbol{\nu} = \boldsymbol{P}^{-T}(\boldsymbol{\rho})\widetilde{\boldsymbol{\tau}} \quad (18)$$

$$\widehat{\boldsymbol{M}}_{ee}\ddot{\widetilde{\mathbf{q}}}_e + \mathbf{D}_{ee}\dot{\widetilde{\mathbf{q}}}_e + \mathbf{K}_{ee}\widetilde{\mathbf{q}}_e = - [C_1\boldsymbol{J}_{1e}\ C_2\boldsymbol{J}_{2e}]^T\widetilde{\boldsymbol{\tau}} \quad (19)$$

where $\widetilde{\boldsymbol{\tau}} \triangleq \widehat{\boldsymbol{\tau}} - \widehat{\boldsymbol{\tau}}_d$ and $\widetilde{\mathbf{q}}_e = \mathrm{col}\{\widetilde{\mathbf{q}}_{1e}, \widetilde{\mathbf{q}}_{2e}\} \triangleq \mathbf{q}_e - \mathbf{q}_{ed}$.

Now consider the function

$$S_\mu = \tfrac{1}{2}\widetilde{\boldsymbol{\nu}}_r^T\boldsymbol{M}\widetilde{\boldsymbol{\nu}}_r + \tfrac{1}{2}(1-\mu)\left[\dot{\widetilde{\mathbf{q}}}_e^T\widehat{\boldsymbol{M}}_{ee}\dot{\widetilde{\mathbf{q}}}_e + \widetilde{\mathbf{q}}_e^T\boldsymbol{K}_{ee}\widetilde{\mathbf{q}}_e\right] \quad (20)$$

which is nonnegative if $\mu < 1$. Its time derivative yields, after substituting for the error dynamics,

$$\dot{S}_\mu = (\widehat{\boldsymbol{\tau}} - \widehat{\boldsymbol{\tau}}_d)^T\mathbf{s}_\mu - (1-\mu)\dot{\widetilde{\mathbf{q}}}_e^T\mathbf{D}_{ee}\dot{\widetilde{\mathbf{q}}}_e. \quad (21)$$

Integrating with respect to time from zero to $T > 0$ and taking $S_\mu(0) = 0$ yields $\int_0^T(\widehat{\boldsymbol{\tau}} - \widehat{\boldsymbol{\tau}}_d)^T\mathbf{s}_\mu\,dt = S_\mu(T) + (1-\mu)\int_0^T\dot{\widetilde{\mathbf{q}}}_e^T\mathbf{D}_{ee}\dot{\widetilde{\mathbf{q}}}_e\,dt$ which suggests that the mapping $\mathbf{s}_\mu = \boldsymbol{G}[\widehat{\boldsymbol{\tau}} - \widehat{\boldsymbol{\tau}}_d]$ embodied by (18), (19), (15), and $\dot{\widetilde{\boldsymbol{\rho}}}_\mu = \dot{\widetilde{\boldsymbol{\rho}}} - (1-\mu)[C_1\boldsymbol{J}_{1e}\dot{\widetilde{\mathbf{q}}}_{1e} + C_2\boldsymbol{J}_{2e}\dot{\widetilde{\mathbf{q}}}_{2e}$ is passive [11] if $\mu < 1$. On the basis of the passivity theorem [11], $\mathbf{s}_\mu \in \boldsymbol{L}_2$ if $\widehat{\boldsymbol{\tau}} - \widehat{\boldsymbol{\tau}}_d = -\boldsymbol{H}[\mathbf{s}_\mu]$ and $\boldsymbol{H}$ is a strictly passive operator, *i.e.*, $\int_0^T\mathbf{s}_\mu^T\boldsymbol{H}[\mathbf{s}_\mu]\,dt \geq \epsilon\int_0^T\mathbf{s}_\mu^T\mathbf{s}_\mu\,dt$, $\forall T > 0$, $\forall\mathbf{s}_\mu \in \boldsymbol{L}_{2e}$, and some $\epsilon > 0$. (If $\epsilon = 0$, $\boldsymbol{H}$ is a passive operator.)

Now, let us replace the parameters in the feedforward in (16) with estimates $\widehat{\mathbf{a}}(t)$ and motivated by the passivity theorem use a positive-definite feedback gain matrix $\mathbf{K}_d = \mathbf{K}_d^T > \mathbf{O}$ for $\boldsymbol{H}$:

$$\widehat{\boldsymbol{\tau}} = \boldsymbol{P}^T\boldsymbol{W}(\dot{\boldsymbol{\nu}}_r, \boldsymbol{\nu}_r, \boldsymbol{\nu})\widehat{\mathbf{a}}(t) - \mathbf{K}_d\mathbf{s}_\mu. \quad (22)$$

Hence,

$$-\int_0^T(\widehat{\boldsymbol{\tau}} - \widehat{\boldsymbol{\tau}}_d)^T\mathbf{s}_\mu\,dt = -\int_0^T\widetilde{\mathbf{a}}^T\boldsymbol{W}^T\boldsymbol{P}\mathbf{s}_\mu\,dt + \int_0^T\mathbf{s}_\mu^T\mathbf{K}_d\mathbf{s}_\mu\,dt.$$

The operator $\boldsymbol{H}$ will be strictly passive if $\widetilde{\mathbf{a}}$ is a passive function of $-\boldsymbol{W}^T\boldsymbol{P}\mathbf{s}_\mu$. The simplest such function if knowledge of the true parameters is to be avoided is an integrator. Therefore,

$$\dot{\widetilde{\mathbf{a}}} = \dot{\widehat{\mathbf{a}}} = -\boldsymbol{\Gamma}\boldsymbol{W}^T(\dot{\boldsymbol{\nu}}_r, \boldsymbol{\nu}_r, \boldsymbol{\nu})\boldsymbol{P}(\boldsymbol{\rho})\mathbf{s}_\mu, \quad (23)$$

$$\boldsymbol{\Gamma} = \boldsymbol{\Gamma}^T > \mathbf{O}$$

The final form of the controller gives us the following:

Theorem. The use of the controller given by (8), (22), (16), and (23) yields $\widetilde{\boldsymbol{\rho}}(t) \to \mathbf{0}$ as $t \to \infty$.

Proof. It has been noted that on the basis of the passivity theorem, $\mathbf{s}_\mu \in \boldsymbol{L}_2$. Now, consider the function

$$V = S_\mu + \tfrac{1}{2}\widetilde{\mathbf{a}}^T\boldsymbol{\Gamma}^{-1}\widetilde{\mathbf{a}} > 0 \ \ (\mu < 1).$$

Using (21), (22), and (23), its time derivative satisfies

$$\dot{V} = -\mathbf{s}_\mu^T\mathbf{K}_d\mathbf{s}_\mu - (1-\mu)\dot{\widetilde{\mathbf{q}}}_e^T\boldsymbol{D}_{ee}\dot{\widetilde{\mathbf{q}}}_e \leq 0.$$

Hence $\mathbf{s}_\mu \in \boldsymbol{L}_2 \cap \boldsymbol{L}_\infty$, $\dot{\widetilde{\mathbf{q}}}_e \in \boldsymbol{L}_2 \cap \boldsymbol{L}_\infty$, $\dot{\widetilde{\boldsymbol{\rho}}}_\mu \in \boldsymbol{L}_2$, $\widetilde{\boldsymbol{\rho}}_\mu \in \boldsymbol{L}_2 \cap \boldsymbol{L}_\infty$, and $\widetilde{\boldsymbol{\rho}}_\mu \to \mathbf{0}$ as $t \to \infty$. Since V is bounded, so are $\widetilde{\mathbf{a}}$ and $\widetilde{\boldsymbol{\nu}}_r$. Since $\mathbf{s}_\mu$, $\dot{\widetilde{\boldsymbol{\rho}}}_\mu$, $\widetilde{\boldsymbol{\rho}}_\mu$, $\dot{\boldsymbol{\rho}}_d$, $\ddot{\boldsymbol{\rho}}_d \to \mathbf{0}$ as $t \to \infty$, so do $\boldsymbol{\nu}_r$ and $\dot{\boldsymbol{\nu}}_r$. Therefore, $\widetilde{\boldsymbol{\tau}} = \widehat{\boldsymbol{\tau}} - \widehat{\boldsymbol{\tau}}_d \to \boldsymbol{P}^T\boldsymbol{W}(\dot{\boldsymbol{\nu}}_r, \boldsymbol{\nu}_r, \boldsymbol{\nu})\widetilde{\mathbf{a}} = \mathbf{0}$. Since $\widetilde{\mathbf{q}}_e$ is the solution of the stable system in (19) with $\widetilde{\boldsymbol{\tau}} \to \mathbf{0}$, then $\widetilde{\mathbf{q}}_e \to \mathbf{0}$. When this result is combined with $\widetilde{\boldsymbol{\rho}}_\mu \to \mathbf{0}$, then $\widetilde{\boldsymbol{\rho}} \to \mathbf{0}$. □

5. Numerical Example

Simulation results will now be presented for a system of two planar arms each with three joints that manipulate a shared object (Figure 2). Each arm has two flexible links and a third rigid link which is cantilevered to the large rigid payload. Bodies $\mathcal{B}_1$, $\mathcal{B}_2$, $\mathcal{B}_4$, and $\mathcal{B}_5$ are modelled as an inboard rigid body, a homogeneous, isotropic flexible beam exhibiting in-plane bending (with bending stiffness EI), and an outboard rigid body. The mass properties of each body are presented in Table 1 where m, c, and J are the zeroth, first,

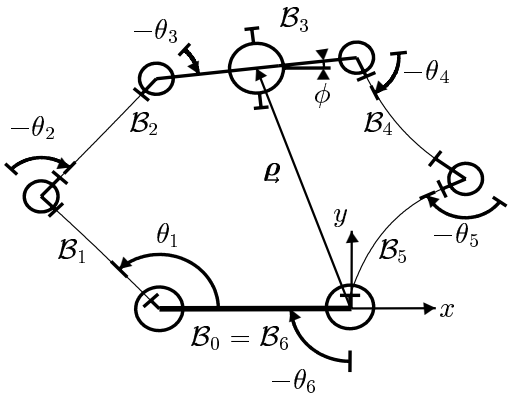

Figure 2: System for Simulation

and second moments of mass relative to the inboard attachment point of the sub-body and ℓ is its length. The geared actuators exhibit a lumped rotor inertia each of which is given in Table 2.

This is a mathematical model of an experimental testbed constructed in the Department of Mechanical Engineering at the University of Canterbury in Christchurch, New Zealand. An analysis of the system vibration modes and both experimental and simulation results for the nonadaptive form of the controller presented in this paper ($\widehat{\mathbf{a}} = \mathbf{a}$ in (22)) is presented in [8]. The close agreement demonstrated there suggests that the simulation results given here for the adaptive case are indicative of what would be achieved in experiment. Other details concerning the modelling procedure and the simulation of the *exact* motion equations (no large payload approximation) subject to the loop-closure constraint are discussed in [8].

The desired trajectory is a circle for the centre of the payload with constant orientation. The centre of the circle is given by $\boldsymbol{\rho}_c = [-0.3 \quad 0.75 \quad 0]^T$ m and its radius is $r_c = 0.15$ m. The payload position around the circle is measured with the angle $\psi(t)$ with $\psi = 0$ corresponding to the "3 o'clock" position. This angle is selected so that the first semicircle is an acceleration phase with $\psi(0) = \pi/2$ (roughly the position in Figure 2), $\dot{\psi}(0) = \ddot{\psi}(0) = 0$, $\dot{\psi}(T) = 2\pi/T$, and $\ddot{\psi}(T) = 0$ with $\psi(t) = (\pi/2) + (\pi t/T) - \sin(\pi t/T)$. The next three full circles are performed with constant angular velocity $\dot{\psi} = 2\pi/T$. The last semicircle is a deceleration phase terminating with $\psi(5T) = \pi/2$ and $\dot{\psi}(5T) = \ddot{\psi}(5T) = 0$, with $\psi(5T - t) = \pi - \psi(t)$, $0 \le t \le T$.

For the following study, $T = 4$ sec., $\mu = 0.8$, $\boldsymbol{\Lambda} = \Omega_c \mathbf{1}$ in (15), and $\mathbf{K}_d = \Omega_c \cdot \boldsymbol{P}(\boldsymbol{\rho}_c)^T \boldsymbol{M} \boldsymbol{P}(\boldsymbol{\rho}_c)$ in (22), where $\Omega_c = 4$ rad/s. The value of $\boldsymbol{\Gamma}$ in the adaptation law is selected to be diagonal with entries

Table 1: Robot Mass Properties

	ℓ (m)	m (kg)	c (g·m)	J (g·m^2)	EI (N·m^2)
Base ($\mathcal{B}_0 = \mathcal{B}_6$)	0.600				
Arm 1					
$\mathcal{B}_1$ rotor	0.037	2.66	1.84	0.23	
$\mathcal{B}_1$ link	0.406	0.20	40.4	10.9	39.3
$\mathcal{B}_1$ stator	0.062	1.92	112.	8.43	
$\mathcal{B}_2$ rotor	0.082	1.80	15.8	2.19	
$\mathcal{B}_2$ link	0.360	0.18	32.3	7.76	39.3
$\mathcal{B}_2$ stator	0.067	0.93	54.6	4.15	
Payload ($\mathcal{B}_3$)	0.598	15.7	4670	1950	
Arm 2					
$\mathcal{B}_4$ rotor	0.067	0.93	7.99	1.02	
$\mathcal{B}_4$ link	0.327	0.19	26.1	9.69	39.3
$\mathcal{B}_4$ stator	0.112	2.10	206.	24.3	
$\mathcal{B}_5$ rotor	0.077	2.23	10.2	3.26	
$\mathcal{B}_5$ link	0.390	0.16	37.3	5.69	39.3
$\mathcal{B}_5$ stator	0.037	2.53	92.5	131.	

Table 2: Rotor Inertias

joint	(g·m^2)	(g·m^2)
1, 6	128.	128.
2, 5	150.	307.
3, 4	16.1	16.1

given by $\Gamma_{mm} = 4\Omega_c T \widehat{\Gamma}_{mm}$ where

$$\begin{aligned} \widehat{\Gamma}_{mm} &= \left[\int_0^T \boldsymbol{W}(\dot{\boldsymbol{\nu}}_d, \boldsymbol{\nu}_d, \boldsymbol{\nu}_d) \mathbf{K}_d^{-1} \right. \\ &\times \left. \boldsymbol{W}(\dot{\boldsymbol{\nu}}_d, \boldsymbol{\nu}_d, \boldsymbol{\nu}_d)\, dt \right]_{mm} . \end{aligned}$$

Given the planar nature of the problem $\mathbf{a}$ effectively contains 4 parameters: m, c_x, c_y, and J_{zz}. For simplicity, we take $\boldsymbol{\rho}_{\mu d} \doteq \boldsymbol{\rho}_d$ so that (17) is not used.

Initially, the control law was implemented using only the feedback portion ($\widehat{\mathbf{a}} \equiv \mathbf{0}$) with balanced load-sharing ($C_1 = C_2 = 0.5$). The resulting tracking performance is illustrated in Figure 3 with large position and orientation errors in evidence. When the feedforward was implemented using the true known parameters ($\widehat{\mathbf{a}} \equiv \mathbf{a}$), the tracking performance illustrated in Figure 4 was obtained with corresponding errors and orientation given in Figure 5. There is considerable improvement over the results using PD feedback alone

with simultaneous vibration suppression.

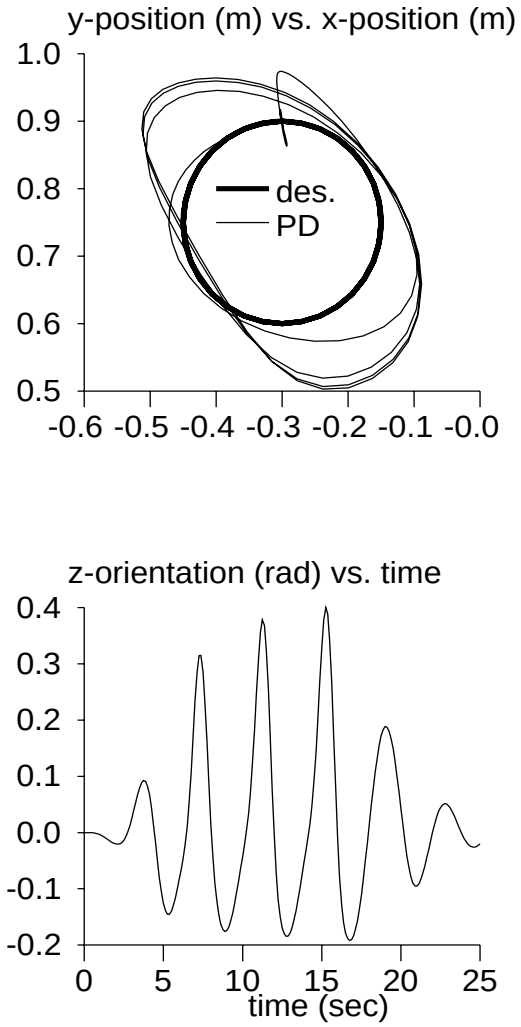

Figure 3: Simulation Results for PD Feedback Control

The results corresponding to the use of the adaptation law in (23) with $\widehat{\mathbf{a}}(0) = \mathbf{0}$ are shown in Figure 5 for two different load-sharing scenarios. Interestingly, they are significantly better than the fixed (known) parameter case which occurs because the feedforward is based on the payload alone. The adaptive form evidently has the ability to account for the "missing" mass in the arms. The evolution of three of the four parameter estimates is shown in Figure 6. As might be expected, the parameters do not converge to the true payload values but larger values indicative of the entire robot.

6. Conclusions

A passivity-based adaptive controller has been developed for two flexible robot arms which manipulate a large rigid payload. The underlying passivity property depends only on the size of the payload and hence is robust with respect to the stiffness properties of the link and the number of modelled modes. A free load-sharing parameter permits the required joint torques to be shared between the arms in an arbitrary fashion.

The robotic system used in the numerical example exhibited significant departures from the assumed payload-dominated model: the payload mass is on the order of that of the two robot arms and the joints exhibit significant rotor inertias. In spite of these effects, the adaptive controller worked quite well.

References

[1] Slotine, J.–J.E. and Li, W., On the Adaptive Control of Robot Manipulators, *Int. J. Rob. Research* 6, 49–59, 1987.

[2] Ortega, R., Loría, A., Nicklasson, P. J., and Sira–Ramírez, H., *Passivity-Based Control of Euler-Lagrange Systems*, Springer–Verlag, London, 1998.

[3] Wang, D. and Vidyasagar, M., Passive Control of a Stiff Flexible Link, *Int. J. Rob. Research* 11, 572–578, 1992.

[4] Damaren, C. J., Passivity Analysis for Flexible Multilink Space Manipulators, *J. Guidance, Control, and Dynamics* 18, 272–279, 1995.

[5] Damaren, C. J., Approximate Inverse Dynamics and Passive Feedback for Flexible Manipulators with Large Payloads, *IEEE Trans. Robotics and Automation* 12, 131–138, 1996.

[6] Damaren, C. J., Adaptive Control of Flexible Manipulators Carrying Large Uncertain Payloads, *J. of Robotic Systems* 13, 219–228, 1996.

[7] Christoforou, E. G. and Damaren, C. J., The Control of Flexible-Link Robots Manipulating Large Payloads: Theory and Experiments, *J. of Robotic Systems*, To appear, 2000.

[8] Damaren, C. J., On the Dynamics and Control of Flexible Multibody Systems with Closed Loops, *Int. J. Rob. Research* 19, 238-253, 2000

[9] Krishnamurthy, K., and Yang, L., Dynamic Modeling and Simulation of Two Cooperating Structurally-Flexible Robotic Manipulators, *Robotica* 13, 375-384, 1995

[10] Matsuno, F. and Hatayama, M., Robust Cooperative Control of Two Two-Link Flexible Manipulators on the Basis of Quasi-Static Equations, *Int. J. Rob. Research* 18, 414–428, 1999.

[11] Desoer, C. A. and Vidysagar, M., *Feedback Systems: Input-Output Properties*, Academic Press, New York, 1975.

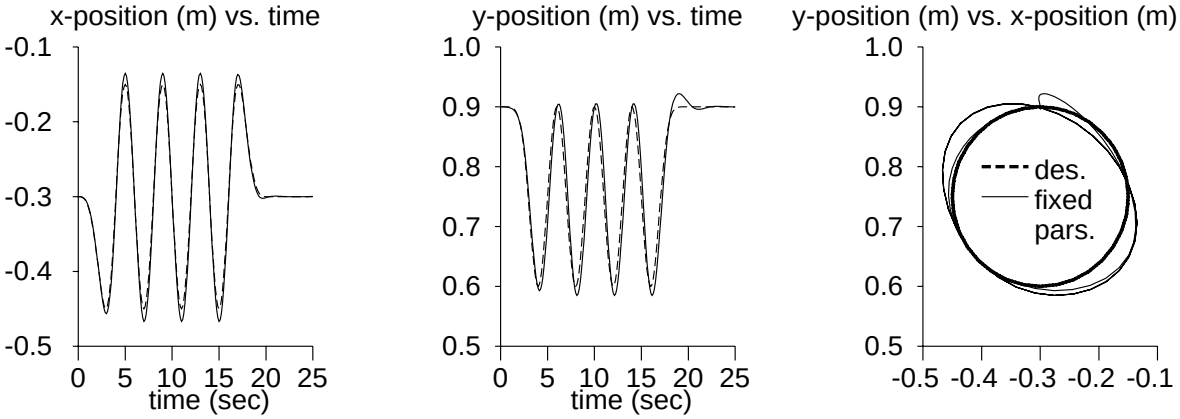

Figure 4: Fixed Parameter Results

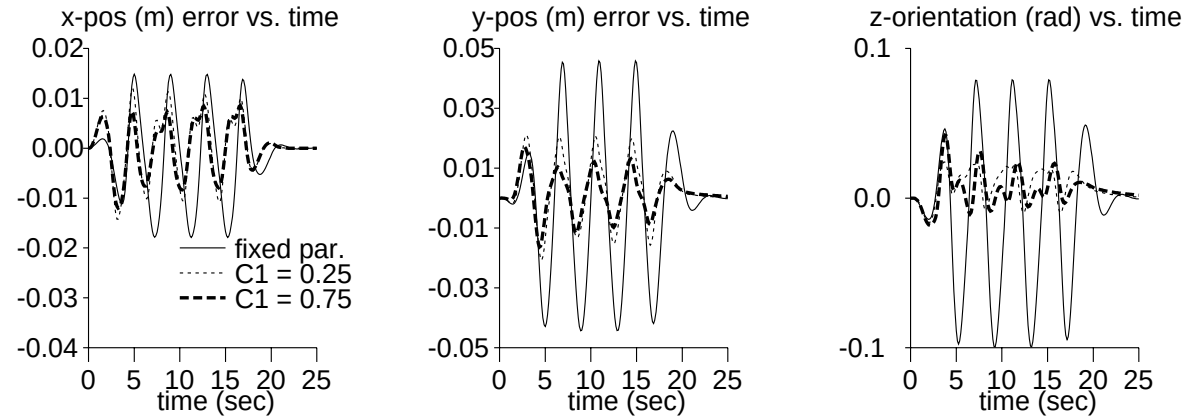

Figure 5: Tracking Errors

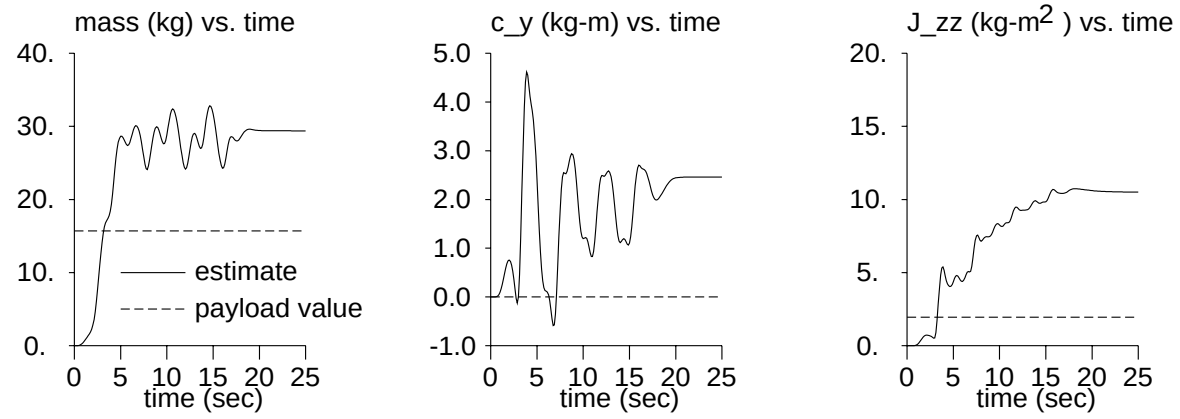

Figure 6: Parameter Estimates